Localized light orbitals: Basis states for three-dimensional optical micro-circuits

2006 Europhys. Lett. 76 222

(http://iopscience.iop.org/0295-5075/76/2/222)

EUROPHYSICS LETTERS 15 October 2006

Europhys. Lett., **76** (2), pp. 222–228 (2006)
DOI: 10.1209/epl/i2006-10252-0

Localized light orbitals: Basis states for three-dimensional optical micro-circuits

H. Takeda, A. Chutinan and S. John

Department of Physics, University of Toronto - 60 St. George St. Toronto, Ontario, M5S 1A7, Canada

received 23 May 2006; accepted in final form 21 August 2006
published online 8 September 2006

PACS. 42.70.Qs – Photonic bandgap materials.
PACS. 42.25.Bs – Wave propagation, transmission and absorption.
PACS. 71.15.-m – Methods of electronic structure calculations.

Abstract. – We demonstrate the method of three-dimensional (3D) optical Wannier functions (WFs) for quantitative description of electromagnetic wave localization and propagation in 3D photonic band gap (PBG) micro-circuits. Using these localized "light orbitals" we accurately reconstruct electromagnetic flow in bulk 3D PBG materials, 2D-3D PBG heterostructures and 2D membrane photonic crystals. The localized orbitals provide a more efficient basis than those used in plane-wave expansions and finite-difference time-domain methods. In 3D photonic crystal circuits, using twenty or fewer WFs, we accurately recapture electromagnetic phenomena over a significant spectral bandwidth surrounding the PBG.

Localized basis states for electronic wave functions are widely used in solid-state physics [1–3]. They provide the foundation for tight-binding model Hamiltonians that describe a rich variety of electronic properties of materials. The localization of electromagnetic waves in disordered structures [4] and photonic band gap materials [5,6] has suggested the possibility of analogous basis states for light. Up to now, the use of optical Wannier functions (WFs) has focused on idealized two-dimensional (2D) photonic crystals where the electric field vector is always perpendicular to the plane of periodicity (TM modes) [7,8]. In this case the localized basis states reduce to scalar wave functions. In 3D periodic microstructures, the full vector nature of the electric and magnetic fields becomes essential. Moreover, induced surface charge and current densities on material interfaces lead to corresponding discontinuities in these vector fields and their derivatives. As a result of these complications, a demonstration of 3D localized light orbitals for guiding light in photonic band gap (PBG) microchips has been lacking.

In this letter, we demonstrate that with typically fewer than twenty 3D localized light orbitals per unit cell, it is possible to precisely recapture electromagnetic effects in bulk 3D PBG materials [9], 2D-3D heterostructures [10,11], and 2D photonic crystal (PC) membranes [12]. 3D optical WFs provide a powerful, and precise computational tool for describing light flow in large-scale optical circuits, in which plane-wave expansion (PWE) [13] and finite-difference time-domain (FDTD) methods [14] become prohibitively cumbersome. The 3D optical WF method achieves computational efficiency by accurately mapping electromagnetic effects in

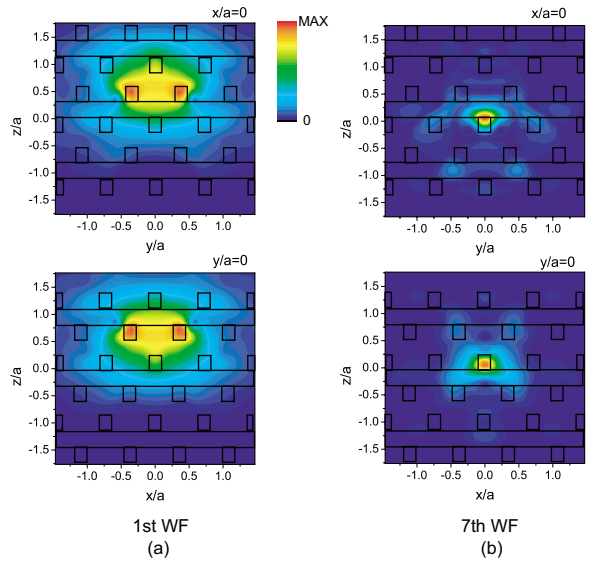

Fig. 1 – Absolute values of the 1st and 7th MLWFs of magnetic fields in a silicon 3D PBG woodpile structure. The rod width is $0.25a$ and the rod height is $0.3a$, where a is the lattice periodicity in the xy plane. Upper and lower figures of each MLWF indicate the distributions in the yz and xz planes, respectively.

the PBG spectral range to an effective one-dimensional tight-binding Hamiltonian. We derive the modification in 3D localized vector orbitals required to treat electric-field discontinuities resulting from modified surface polarization charges near defects in PCs.

Consider a bulk periodic 3D PBG structure, with the magnetic-field Bloch functions, $\boldsymbol{H}^{(0)}_{n\boldsymbol{k}}(\boldsymbol{r})$, band index n and Bloch wave vector $\boldsymbol{k}$. We construct maximally localized WFs (MLWFs), from linear combinations of Bloch functions of the form $\boldsymbol{H}_{n\boldsymbol{k}}(\boldsymbol{r}) = \sum_{m=1}^{N} U^{(\boldsymbol{k})}_{mn} \boldsymbol{H}^{(0)}_{m\boldsymbol{k}}(\boldsymbol{r})$, where $U^{(\boldsymbol{k})}_{mn}$ is an arbitary unitary matrix defined for each $\boldsymbol{k}$ point, and N is the number of photonic bands. A general (unoptimized) WF of the magnetic field centered at lattice vector $\boldsymbol{R}$, is defined as $\boldsymbol{W}^{(\boldsymbol{H})}_{n\boldsymbol{R}}(\boldsymbol{r}) = \frac{1}{N_{\boldsymbol{k}}} \sum_{\boldsymbol{k}} e^{-i\boldsymbol{k}\cdot\boldsymbol{R}} \boldsymbol{H}_{n\boldsymbol{k}}(\boldsymbol{r})$, where the $\boldsymbol{k}$ summation spans the first Brillouin zone (BZ) and $N_{\boldsymbol{k}}$ is the number of discrete points in the first BZ. When the WFs of the magnetic fields are chosen purely real, the corresponding electric-field WFs $\boldsymbol{W}^{(\boldsymbol{E})}_{n\boldsymbol{R}}(\boldsymbol{r})$, obtained from Maxwell's equation are purely imaginary.

A variety of different localized light orbitals can be constructed depending on the choice of $U^{(\boldsymbol{k})}_{mn}$. Following the analogy with electronics [2,3], MLWFs of the magnetic field are constructed by finding the unitary transformation $U^{(\boldsymbol{k})}_{mn}$ that minimizes the spatial spread of the localized orbital:

$$\Omega = \sum_{n=1}^{N} \left[\left\langle \boldsymbol{W}^{(\boldsymbol{H})}_{n\boldsymbol{0}} | \boldsymbol{r}^2 | \boldsymbol{W}^{(\boldsymbol{H})}_{n\boldsymbol{0}} \right\rangle - \left(\left\langle \boldsymbol{W}^{(\boldsymbol{H})}_{n\boldsymbol{0}} | \boldsymbol{r} | \boldsymbol{W}^{(\boldsymbol{H})}_{n\boldsymbol{0}} \right\rangle \right)^2 \right]. \tag{1}$$

The spread functional is minimized using an iterative method described in the context of electronics [2,3] using initial trial WFs that exhibit symmetries of the corresponding Bloch modes at $\boldsymbol{k} = \boldsymbol{0}$ and that are centered at various high-symmetry points of the unit cell. This leads to the most efficient basis. For example in the silicon woodpile of fig. 1, the initial

trial WFs are the $\boldsymbol{k} = \boldsymbol{0}$ Bloch modes, modulated by tightly localized Gaussian functions $\exp[-(x-x^{(n)})^2/\sigma_x^2]\exp[-(y-y^{(n)})^2/\sigma_y^2]\exp[-(z-z^{(n)})^2/\sigma_z^2]$, with $\sigma_x = \sigma_y = 0.3a$, $\sigma_z = 0.8c$, where $c = 1.2a$, and the center points $(x^{(n)}, y^{(n)}, z^{(n)})$ for the first 12 functions chosen from the set of $(0,0,c/2)$, $(0,0,0)$, $(0,0,0)$, $(0,0,0)$, $(0.5a,0.5a,0)$, $(0.5a,0.5a,0)$, $(0,0,0)$, $(0,0,0)$, $(0.5a,0,0)$, $(0,0.5a,0)$, $(0,0,0)$ and $(0,0,0)$.

In the presence of a dielectric defect, $\delta\epsilon(\boldsymbol{r})$, over and above the periodic dielectric function $\epsilon_p(\boldsymbol{r})$, the electric-field Maxwell wave equation ensuring the absence of free charges, $\nabla\cdot\{\epsilon(\boldsymbol{r})\boldsymbol{E}(\boldsymbol{r})\} = 0$, where $\epsilon(\boldsymbol{r}) = \epsilon_p(\boldsymbol{r}) + \delta\epsilon(\boldsymbol{r})$, must be satisfied. In scalar wave WF theory [2,3,7,8], the electric field near such a defect is expanded in the basis of unperturbed functions $\boldsymbol{W}_{n\boldsymbol{R}}^{(\boldsymbol{E})}(\boldsymbol{r})$. However, for a general 3D electromagnetic vector field, the modified distribution of surface polarization charges cannot be represented by WFs constructed to describe the original surface charge distribution: $\nabla\cdot\{\epsilon_p(\boldsymbol{r})\boldsymbol{W}_{n\boldsymbol{R}}^{(\boldsymbol{E})}(\boldsymbol{r})\} = 0$. To address this important issue, we convert (using Maxwell equations) the magnetic-field WFs to electric-field WFs. In order to represent the induced polarization charge of the defect and enforce the condition that the defect does not introduce any free charge carriers, we write: $\boldsymbol{E}(\boldsymbol{r}) = \sum_{n\boldsymbol{R}} E_{n\boldsymbol{R}}\tilde{\boldsymbol{W}}_{n\boldsymbol{R}}^{(\boldsymbol{E})}(\boldsymbol{r})$, where $\tilde{\boldsymbol{W}}_{n\boldsymbol{R}}^{(\boldsymbol{E})}(\boldsymbol{r}) = \boldsymbol{W}_{n\boldsymbol{R}}^{(\boldsymbol{E})}(\boldsymbol{r}) - \nabla\phi_{n\boldsymbol{R}}(\boldsymbol{r})$. Here $\phi_{n\boldsymbol{R}}(\boldsymbol{r})$ is a scalar potential satisfying the Poisson equation for a hypothetical periodic dielectric $\tilde{\epsilon}(\boldsymbol{r}) \equiv \epsilon_p(\boldsymbol{r}) + \delta\epsilon_p(\boldsymbol{r})$, $\delta\epsilon_p(\boldsymbol{r}) \equiv \sum_{\boldsymbol{R}}\delta\epsilon(\boldsymbol{r}+\boldsymbol{R})$:

$$\nabla\cdot\{\tilde{\epsilon}(\boldsymbol{r})\nabla\phi_{n\boldsymbol{R}}(\boldsymbol{r})\} = \nabla\cdot\left\{\delta\epsilon_p(\boldsymbol{r})\boldsymbol{W}_{n\boldsymbol{R}}^{(\boldsymbol{E})}(\boldsymbol{r})\right\}. \tag{2}$$

This equation for $\phi_{n\boldsymbol{R}}(\boldsymbol{r})$ is solved in $\boldsymbol{k}$-space, using the known Fourier decompositions of the other functions. With modified expansion of $\boldsymbol{E}(\boldsymbol{r})$, it is then straightforward to verify that the electric field satisfies the divergence condition including defects even though $\boldsymbol{W}_{n\boldsymbol{R}}^{(\boldsymbol{E})}(\boldsymbol{r})$ obey the divergence condition for the purely periodic PC. The right side in eq. (2) corresponds to a polarization charge density generated by $\delta\epsilon(\boldsymbol{r})$. We refer to $\boldsymbol{W}_{n\boldsymbol{R}}^{(\boldsymbol{E})}(\boldsymbol{r})$ and $\tilde{\boldsymbol{W}}_{n\boldsymbol{R}}^{(\boldsymbol{E})}(\boldsymbol{r})$ as the unmodified and modified optical WFs, respectively. By substituting the modified expansion of $\boldsymbol{E}(\boldsymbol{r})$ into the electric-field Maxwell's wave equation, we obtain an N-dimensional ($N \leq 20$) tight-binding matrix representation that accurately describes electromagnetic flow through waveguides and point-defect modes as well as transmission and reflection of light within complex 3D PBG circuit paths. In the event that the PC has more than one type of defect, more than one type of modified electric field WF would be required and matrix elements between the different types of WFs would be needed. The detailed evaluation of these 3D WFs and the resulting matrix elements will be presented elsewhere [15].

As a first illustration of the accuracy and efficiency of 3D optical WFs we consider a bulk silicon woodpile 3D PBG structure [16–18]. The dielectric index of Si is $\epsilon = 11.9$ and the width and height of rods are chosen to be $d = 0.25a$ and $h = 0.3a$, respectively, where a is the distance between the centers of neighboring rods. Since one unit cell of the woodpile has 4 stacking layers, the periodicity of stacking layers is $c = 4h = 1.2a$. We take the simple cubic structure $a \times a \times c$ as a unit cell. This structure has a 3D PBG with gap to center frequency ratio of 17.7%. We construct 12 MLWFs of magnetic fields: 4 MLWFs from the first 4 photonic bands below the 3D PBG, and 8 MLWFs from many crossing (entangled) photonic bands above the 3D PBG. In figs. 1(a) and (b), we show the absolute values of MLWFs of magnetic fields for the 1st and 7th MLWFs, respectively. Upper and lower figures of each MLWF indicate the distributions in the yz and xz planes, respectively. The center points of the 1st and 7th MLWFs are $(0,0,c/2)$ and $(0,0,0)$, respectively. The symmetry of each of the MLWFs originates from the symmetry of the corresponding Bloch functions at crystal momentum $\boldsymbol{k} = \boldsymbol{0}$. We have verified that with 12 MLWFs, and the fourth nearest-neighboring matrix elements, it is possible to accurately recapture the bands below $\omega a/2\pi c = 0.48$ of the bulk 3D band structure.

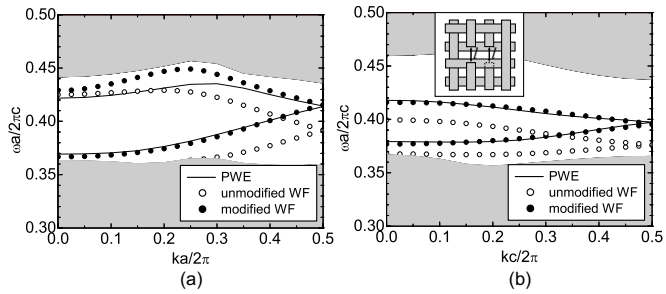

Fig. 2 – Guided modes in the silicon woodpile of fig. 1 in the case of removing (a) one rod and (b) rod segments in the stacking direction. The inset shows a top view of the periodically removed rod segments of length $l = 0.5a$. The solid line, solid and open circles indicate the PWE, modified and unmodified optical WF methods, respectively. Shaded regions indicate the projected photonic band structures.

As a second illustration, we consider two types of waveguides in the 3D woodpile. One consists of removing a single dielectric rod [19, 20]. Another consists of removing a zig-zag pattern of vertically stacked rod segments (vertical waveguide) [21, 22]. Figure 2(a) shows the guided modes in the case of removing one rod. Clearly, the defect polarization charge contained in the modified Wannier orbitals $\tilde{\boldsymbol{W}}^{(\boldsymbol{E})}_{n\boldsymbol{R}}(\boldsymbol{r})$, plays a significant role in obtaining agreement between the PWE method (solid line) with 4375 plane waves (in a $1 \times 4 \times 4$ supercell) and the MLWF method (solid circles) with 12 localized light orbitals. For $\omega a/2\pi c > 0.42$, the modified MLWF ($N = 12$) method overestimates the guided mode frequency. Higher accuracy in this spectral range requires the inclusion of more MLWFs above the 3D PBG [15]. Figure 2(b) describes a single-mode vertical waveguide. The inset shows a top view of the periodically removed rod segments of length $l = 0.5a$. This architecture has been shown [21, 22] to provide high-bandwidth, lossless, interconnection between 2D microchip layers embedded in the 3D woodpile. In fig. 2(b), the modified optical WF can recapture the guided mode precisely. In both cases, the modified optical WF method (solid circles) improves accuracies greatly, compared to the unmodified optical WF (open circles). The computational time required to obtain the guided mode in fig. 2 by modified MLWF is over a factor of 100 less than that required in the PWE supercell. This suggests the scalability of the MLWF method to large-scale optical circuits in a 3D PBG microchip [21].

Another important class of 3D microstructures involve guiding in a 2D planar circuit (xy plane). In 2D membrane PCs [12], confinement in the z-direction occurs through total internal reflection. In 2D-3D PBG heterostructures [10, 11], confinement of light to an intercalated 2D PC micro-chip layer occurs by virtue of the 3D PBG cladding material above and below the planar defect layer. In both cases, periodic boundary conditions are imposed in the z-direction based on the supercell technique. A WF of the magnetic field, centered at lattice vector $\boldsymbol{R}_{||}$, is then defined as $\boldsymbol{W}^{(\boldsymbol{H})}_{n\boldsymbol{R}_{||}}(\boldsymbol{r}_{||}, z) = \frac{1}{N_{\boldsymbol{k}_{||}}} \sum_{\boldsymbol{k}_{||}} e^{-i\boldsymbol{k}_{||}\cdot\boldsymbol{R}_{||}} \boldsymbol{H}_{n\boldsymbol{k}_{||}}(\boldsymbol{r}_{||}, z)$, where $||$ indicates the 2D coordinate, and the summation spans the 2D BZ of the planar microchip. $\boldsymbol{W}^{(\boldsymbol{H})}_{n\boldsymbol{R}_{||}}(\boldsymbol{r}_{||}, z)$ is localized only in the 2D xy plane, and has a periodicity in the z-direction, $\boldsymbol{W}^{(\boldsymbol{H})}_{n\boldsymbol{R}_{||}}(\boldsymbol{r}_{||}, z) = \boldsymbol{W}^{(\boldsymbol{H})}_{n\boldsymbol{R}_{||}}(\boldsymbol{r}_{||}, z + L)$, where L is the vertical length of the supercell.

For concreteness, we consider the 2D-3D PBG heterostructure composed of inverse [001]-diamond:5 square spiral structures [23, 24] inserted with a 2D micro-chip layer with circular rods [10, 11]. The inverse square spiral structure is made from an air coil with a single loop.

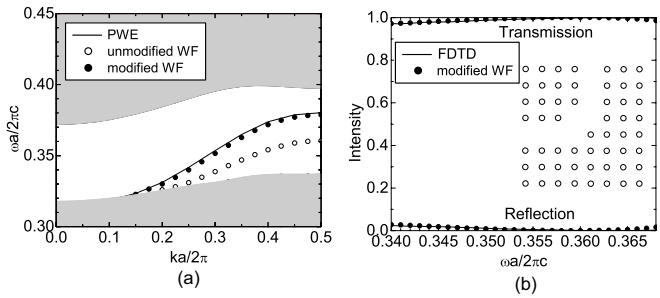

Fig. 3 – (a) Single guided mode in the case of removing one line of rods in a 2D square lattice micro-chip layer intercalated within an inverse square spiral PBG material made of silicon (see text for structural parameters). The solid line, solid and open circles indicate the PWE, modified and unmodified optical WF methods, respectively. Shaded regions indicate the projected photonic band structures. (b) Transmission and reflection spectra in a 90° bent air waveguide. The inset indicates the 90° bent air waveguide. Solid lines and solid circles indicate the FDTD and modified optical WF methods, respectively.

The dielectric index of a background Si is $\epsilon = 11.9$. The [001]-diamond:5 has $[L, c, r] = [1.5, 1.7, 0.33]a$, where L, c, r and a are the transverse arm length, the vertical period, the radius of coated coils and the lattice constant, respectively. The radius of rods in the 2D micro-chip layer is $r_d = 0.17a$, and the thickness of the 2D micro-chip layer is $t = 0.5a$. In the calculation of the 2D-3D PBG heterostructure, we take 4 unit cells of 3D PBG cladding material (2 above and 2 below) in the z-direction. The overall length of a supercell is $L = 4c + t = 7.3a$. With this choice of supercell, there are 16 photonic bands below the PBG, and many crossing (entangled) photonic bands above the PBG. We construct 18 MLWFs: 16 MLWFs from bands below the PBG and 2 MLWFs from above the PBG. We consider a guided mode in the case of removing one line of rods in the 2D micro-chip layer. Figure 3(a) shows the single guided mode. The solid line, solid and open circles and shaded regions are the same as those in fig. 2. As shown in fig. 3(a), the solid circles become close to the solid line, unlike the open circles.

In the 2D-3D PBG heterostructure, we calculate the transmission and reflection spectra in a 90° bent air waveguide in the 2D micro-chip layer. Figure 3(b) shows them in the 90° bent waveguide in the frequency range of $0.34 \leq \omega a/2\pi c \leq 0.368$. The inset indicates the 90° bent air waveguide. Solid lines and solid circles indicate the FDTD and modified optical WF methods, respectively. The solid lines and the solid circles are the same. In the FDTD method, the resolution is 10 grid points per lattice constant, corresponding to 1000 basis functions (delta functions) per unit cell.

In 2D membrane PCs, we consider the triangular-lattice PC composed of circular air holes in a 2D GaAs slab with an air background. The dielectric index of GaAs is $\epsilon = 11.56$ and the radius of air holes is $R/a = 0.29$, where a is the lattice constant. The thickness of the 2D membrane is $t = 0.6a$. The overall length of a supercell with the 2D membrane and air cladding is $L = 4a$. Only light that satisfies the condition of total internal reflections is confined strictly to propagate within the 2D membrane PCs. The region of frequencies and wave vectors in which light leaks into the external air background is called the light cone. This 2D membrane PC has a large in-plane PBG in the even mode of $H_z(\boldsymbol{r}_{||}, z) = H_z(\boldsymbol{r}_{||}, -z)$.

We construct 12 MLWFs. In figs. 4(a) and (b), the absolute values of the magnetic field for the 1st and 7th MLWFs are shown. Upper and lower figures of each MLWF indicate

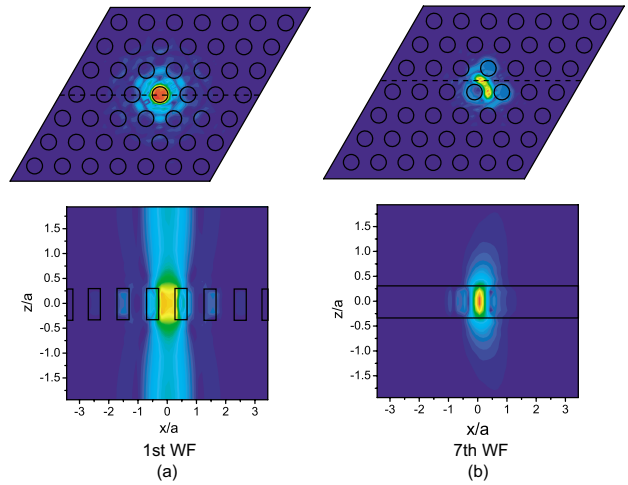

Fig. 4 – Absolute values of 1st and 7th MLWFs of magnetic fields in $0.6a$ thick 2D membrane PC consisting of triangular lattice of air holes of radius $0.29a$ in a dielectric background of 11.56. Upper and lower figures of each MLWF indicate the distributions at $z = 0$ and at certain y described by dashed lines in the upper figures, respectively.

the distributions at $z = 0$ and at certain y described by dashed lines in the upper figures, respectively. The 2D membrane PC is confined to the slab region $|z| < 0.3a$.

We consider guided modes in the PC membrane for the case of missing line of air holes. Figures 5(a) and (b) show the guided modes in the unmodified and modified optical WF methods, respectively. Solid lines and light shaded regions are waveguide modes (PWE) and 2D PC bands, respectively. Dark shaded regions indicate the light cone. Solid circles indicate the optical WF method. In fig. 5(a) the solid lines and the solid circles (unmodified WFs) do not coincide at all. In fig. 5(b), on the other hand, the solid lines and the solid circles (modified WFs) converge.

In conclusion, we have demonstrated the efficacy of 3D optical WF method to a broad variety of 3D periodic dielectric microstructures with planar, line, and point defects. The key insight in efficiently obtaining a precise description of electromagnetic flow in these struc-

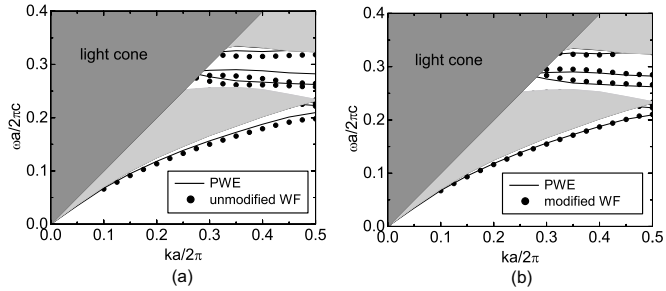

Fig. 5 – Guided modes for membrane PC of fig. 4 in the case of missing line of air holes in the even mode of $H_z(\boldsymbol{r}_{||}, z) = H_z(\boldsymbol{r}_{||}, -z)$: (a) unmodified and (b) modified optical WF methods. The solid line and solid circles indicate the PWE and optical WF methods, respectively. Light shaded regions indicate the projected photonic band structures. Dark shaded regions indicate the light cone.

tures is the modification of MLWFs to accommodate the polarization charge densities created by defects. This creates discontinuities in the electromagnetic field vectors, not previously encountered in scalar wave calculations [2, 3, 7, 8]. Using less than twenty modified optical WFs and two orders of magnitude less computational time, we obtain high accuracies for guided modes, compared to the PWE supercell and FDTD methods. These results suggest that 3D localized light orbitals provide a novel and reliable method for describing realistic electromagnetic effects in 3D PBG microchips, with scalability to very large optical circuits.

* * *

We are grateful to Prof. K. Busch, Dr S. F. Mingaleev and M. Schillinger for valuable discussions about 2D TM WFs. This work was supported in part by the Natural Sciences and Engineering Research Council of Canada and the Ontario Premier's Platinum Research Prize.

REFERENCES

[1] Wannier G. H., *Phys. Rev.*, **52** (1937) 191.
[2] Marzari N. and Vanderbilt D., *Phys. Rev. B*, **56** (1997) 12847.
[3] Souza I., Marzari N. and Vanderbilt D., *Phys. Rev. B*, **65** (2001) 035109.
[4] John S., *Phys. Rev. Lett.*, **53** (1984) 2169.
[5] John S., *Phys. Rev. Lett.*, **58** (1987) 2486.
[6] Yablonovitch E., *Phys. Rev. Lett.*, **58** (1987) 2059.
[7] Busch K., Mingaleev S. F., Garcia-Martin A., Schillinger M. and Hermann D., *J. Phys. Condens. Matter*, **15** (2003) R1233.
[8] Whittaker D. M. and Croucher M. P., *Phys. Rev. B*, **67** (2003) 085204.
[9] Chutinan A. and Noda S., *Appl. Phys. Lett.*, **75** (1999) 3739.
[10] Chutinan A., John S. and Toader O., *Phys. Rev. Lett.*, **90** (2003) 123901.
[11] Chutinan A. and John S., *Phys. Rev. E*, **71** (2005) 026605.
[12] Chutinan A. and Noda S., *Phys. Rev. B*, **62** (2000) 4488.
[13] Busch K. and John S., *Phys. Rev. E*, **58** (1998) 3896.
[14] Taflove A. and Hagness S. C., *Computational Electrodynamics: The Finite-Difference Time-Domain Method* (Artech House, Boston) 1995.
[15] Takeda H., Chutinan A. and John S., to be published in *Phys. Rev. B*.
[16] Ho K. M., Chan C. T., Soukoulis C. M., Biswas R. and Sigalas M., *Solid State Commun.*, **89** (1994) 413.
[17] Lin S.-Y., Fleming J., Hetherington D., Smith B., Biswas R., Ho K., Sigalas M., Zubrzycki W., Kurtz S. and Bur J., *Nature*, **394** (1998) 251.
[18] Noda S., Tomoda K., Yamamoto N. and Chutinan A., *Science*, **289** (2000) 604.
[19] Sigalas M. M., Biswas R., Ho K. M., Soukoulis C. M., Turner D., Vasiliu B., Kothari S. C. and Lin S., *Microwave Opt. Technol. Lett.*, **23** (1999) 56.
[20] Chutinan A. and Noda S., *Appl. Phys. Lett.*, **75** (1999) 3739.
[21] Chutinan A. and John S., *Phys. Rev. B*, **72** (2005) 161316(R).
[22] Chutinan A. and John S., *Opt. Express*, **14** (2006) 1266.
[23] Toader O. and John S., *Science*, **292** (2001) 1133.
[24] Toader O. and John S., *Phys. Rev. E*, **66** (2002) 016610.